Available online at www.sciencedirect.com
SCIENCE DIRECT
Journal of Computational Physics 216 (2006) 780–801
JOURNAL OF COMPUTATIONAL PHYSICS
www.elsevier.com/locate/jcp

Spectral difference method for unstructured grids I: Basic formulation

Yen Liu [a,*], Marcel Vinokur [b], Z.J. Wang [c,1]

[a] NASA Ames Research Center, Moffett Field, CA 94035, United States
[b] Eloret Corp., Sunnyvale, CA 94087, United States
[c] Department of Aerospace Engineering, Iowa State University, 2271 Howe Hall, Ames, IA 50011, United States

Received 6 May 2005; received in revised form 11 November 2005; accepted 4 January 2006
Available online 2 March 2006

Abstract

A new, high-order, conservative, and efficient method for conservation laws on unstructured grids is developed. It combines the best features of structured and unstructured grid methods to attain computational efficiency and geometric flexibility; it utilizes the concept of discontinuous and high-order local representations to achieve conservation and high accuracy; and it is based on the finite-difference formulation for simplicity. Universal reconstructions are obtained by distributing unknown and flux points in a geometrically similar manner for all unstructured cells. Placements of these points with various orders of accuracy are given for the triangular elements. Accuracy studies of the method are carried out with the two-dimensional linear wave equation and Burgers' equation, and each order of accuracy is verified numerically. Numerical solutions of plane electromagnetic waves incident on perfectly conducting circular cylinders are presented and compared with the exact solutions to demonstrate the capability of the method. Excellent agreement has been found. The method is much simpler than the discontinuous Galerkin and spectral volume methods for unstructured grids.

Keywords: High-order; Conservation laws; Unstructured grids; Spectral difference; Spectral collocation method

1. Introduction

A current problem of great interest is to develop a numerical method for conservation laws with the following properties: that it be (a) conservative, (b) high-order accurate, (c) geometrically flexible, (d) computationally efficient, and (e) simply formulated. Simplicity and computational efficiency can be achieved using structured grids. The earliest and most widely used method is the finite-difference (FD) method employing a body-fitted curvilinear coordinate system [3,37], with the equations written in strong conservation law form [39]. The spatial differencing is essentially one-dimensional, and carried out along coordinate directions. Thus

* Corresponding author. Tel.: +1 650 604 6667; fax: +1 650 604 1095.
E-mail addresses: Yen.Liu@nasa.gov (Y. Liu), zjw@iastate.edu (Z.J. Wang).
[1] Tel.: +1 515 294 1614.

0021-9991/$ - see front matter
doi:10.1016/j.jcp.2006.01.024

a large number of data points are ignored in high-order stencils. Near boundaries, the stencil has to be modified with one-sided formulas. Since numerical grid generators are mostly only second-order accurate, the numerical differencing of grid point coordinates in evaluating metric terms can severely degrade the accuracy of the solution if the grid is not sufficiently smooth. The unknowns are solution values at grid points. Therefore the true integral conservation laws can only be satisfied to second-order accuracy. When a single structured grid is not feasible for very complex geometries, multi-block patched or overlapping grids are employed [4]. At interface boundaries between patches, or in overlapped regions, the high accuracy is generally degraded or sophisticated interface algorithms are needed.

In order to satisfy the integral conservation laws, finite-volume (FV) methods were developed, e.g. [29,19]. The unknowns are now cell averages over quadrilaterals (2D) or hexahedra (3D). A high order reconstruction in terms of neighboring unknowns is used to calculate flux integrals over cell boundaries, using Riemann solvers and appropriate limiters. In practice, the conventional finite-volume method for structured grids does not overcome the limitations of the finite-difference method. The reconstruction is still one-dimensional along coordinate directions. While geometric quantities such as surface area vectors or cell volumes can be precisely calculated, flux integrals and volume integrals are usually evaluated by one-point quadratures, and are only second-order accurate. Both methods suffer significant loss of accuracy for very unsmooth, highly curved grids.

In order to achieve geometric flexibility along with high accuracy, we normally use an unstructured grid consisting of triangles in 2D and tetrahedra in 3D. The most commonly used conservative unstructured method is the finite-volume (UFV) method, applied to the integral form of the conservation law with cell averages of the conservative variables as the unknowns [2,13,26]. A polynomial reconstruction of any desired order of accuracy for each cell is obtained in terms of unknowns at neighboring cells. The flux integral for each face is evaluated using the reconstructed solutions from the two cells sharing the face and an approximate Riemann solver. A quadrature approximation is employed for non-linear flux functions. Thus, conservation is satisfied locally for each cell. However, due to the unstructured nature of the grid, it is difficult to obtain a non-singular stencil [13]. This necessitates a least-squares inversion in general. For very high order of accuracy, the number of cells, and thus the number of operations to carry out the numerical procedure, can become very large in three dimensions. This would hamper the efficiency of the method. Furthermore, since each unknown employs a different stencil, one must repeat the least-squares inversion for every cell at each time step, or must store the inversion coefficients. In a high-order, three-dimensional computation, the former would involve impractically large CPU times, while for the latter the memory requirement becomes prohibitive. In addition, the data from neighboring cells required for the computation can be far apart in memory. This further degrades the efficiency of the method due to data gathering and scattering. As a result of these deficiencies, the UFV method is limited to second-order accuracy in most applications.

An alternate method for unstructured grids is the finite-difference (UFD) method, applied to the differential form of the conservation law with values of the conservative variables at grid nodes as the unknowns [8,1,36]. Actually, one only needs an arbitrary set of nodal points, without the connections that define a grid. Here one employs a local polynomial reconstruction of the fluxes in terms of neighboring values determined by the unknowns. The method is simpler than the UFV method, since one only needs to differentiate the reconstructed solution. However, the UFD method has a major disadvantage of not being locally or globally conservative.

Finite-element (FE) methods [18] have long been used for unstructured grids because of their geometric flexibility. As in the unstructured FV method, the global domain is subdivided into triangular or tetrahedral cells, called elements. A major difference between the FE and FV or FD methods is that in the former we employ reconstruction data from within the element, while in the latter the reconstruction data comes from outside the cell. In the FE formulation, the unknowns are nodal values at nodes which are placed at geometrically similar points in each element. As a result, the local reconstructions become universal for all elements in terms of the same set of cardinal basis functions or shape functions. By assigning a single value to the nodes on element boundaries, a global reconstruction is now piecewise continuous. The conservation equations are then satisfied in a weak form via the method weighted of residuals (MWR), by multiplying the equations with the requisite number of test functions, integrating over the global domain, and using integration by parts. Usually the Galerkin approach is used, in which the test functions are the same as the basis functions. This results in a

set of coupled equations of all unknowns. Their solution involves a very large, sparse matrix, whose entries depend on the element geometries. For non-linear equations, quadrature approximations are necessary to evaluate the matrix entries. While the integral conservation law is satisfied for the global domain, it is not satisfied for each element.

In practice, all the above methods normally employ relatively low-order approximations in their formulations. We now turn to a class of methods called spectral methods which have the properties of very high accuracy and spectral (or exponential) convergence [14,5]. In traditional spectral methods, the unknown variable is expressed as a truncated series expansion in terms of some basis functions (trial functions) and solved using the MWR. The trial functions are infinitely differentiable global functions, and the most frequently used ones are trigonometric functions or Chebyshev and Legendre polynomials. In the spectral Galerkin method the test functions are the same as the trial functions, while in the spectral collocation method they are the translated Dirac delta functions centered at so-called collocation points. There are two types of formulations. In the modal formulation, the unknowns are the expansion coefficients. In contrast, for the nodal formulation, the unknowns are the nodal values of the unknown variables at the collocation points. For the Galerkin method, one can use either formulation. However, since the test functions and the trial functions are in general orthogonal to each other only in the modal space, the modal formulation will result in an uncoupled system, but not in the nodal formulation. For the collocation method, the nodal formulation is the more natural choice, and it always results in an uncoupled system since the delta functions are used as the test functions. For nonlinear fluxes, the pseudo-spectral method [30] is commonly used for computational efficiency, in which fluxes are calculated at nodal points using the nodal values of unknowns. For the modal formulation, this requires that unknowns and possibly their derivatives be first transferred to the nodal space, and then fluxes are transferred back to the modal space to compute their derivatives. While the original formulations were carried out in one dimension, their tensor products can be employed for problems in a simple multi-dimensional rectangle or box.

One of the major shortcomings of the traditional spectral methods is their restriction to problems in simple domains. Recent developments have extended these methods to multiple domains, including the spectral element (SE) method [31,25] based on the Galerkin approach and the multi-domain spectral method [21–24,16] based on the collocation approach. Domains containing general quadrilateral and hexahedral elements can be handled by mapping the general elements to the standard elements using the conventional iso-parameterization. The SE method has also been extended to triangular and tetrahedral elements [20].

The SE method can be viewed as a high-order FE method with the nodal points placed at proper locations so that the spectral convergence can be obtained. In order to achieve local conservation for the FE or SE methods, the discontinuous Galerkin (DG) method was developed [32,9–12,17]. Nodes on element boundaries are allowed to have multiple values, so that the local reconstruction in each element is in general discontinuous with that of its neighbors. The Galerkin MWR method is now applied locally to each element, using the local shape functions. As in the unstructured FV method, a Riemann solver is employed at element boundaries to compute the numerical fluxes. The integral conservation law is now satisfied for each element. While we must still solve a large set of coupled equations, each set involves only the unknowns in a few neighboring elements. Some of the integrals in the matrix entries involve quadratic terms. For non-linear flux functions, the required quadrature formulas must have twice the degree of precision as the precision of the reconstruction. In order to obtain stable and spectral convergence, unknowns for the DG method are normally placed at points where the reconstruction matrix is optimized. One choice involves the Fekete points where the determinant of the reconstruction matrix is maximized [38]. Other choices include points where the maximum Lebesgue constant of the reconstruction matrix is minimized [6,7] or multivariate point sets through the electrostatic analogy [15]. In general, these points may not provide the necessary precisions of quadrature approximations for the surface and volume integrals, and one must therefore obtain solutions at other quadrature points through interpolations.

The universal local reconstruction concept inherent in the FE method can be utilized to overcome the computational inefficiencies of the more direct unstructured FV method. In the spectral volume (SV) method [40–43,28], each triangular or tetrahedral cell, here called a spectral volume (SV), is partitioned into structured subcells called control volumes (CV). These are polygons in 2D, and polyhedra in 3D. The latter can have non-planar faces, which must be subdivided into planar facets in order to perform flux integrations. The

unknowns are now cell averages over the CV's. If the SV's are partitioned in a geometrically similar manner, a single, universal reconstruction results. Thus only a few coefficients need to be stored in advance to evaluate all flux integrals. For high orders of accuracy in 3D, the partitioning requires the introduction of a large number of parameters, whose optimization to achieve spectral convergence becomes increasingly more difficult. The growth in the number of interior facets and the increase in the number of quadrature points for each facet, raises the computational cost greatly. The computational cost of the SV method, and the difficulties in determining the parameters for spectral convergence, can both be significantly reduced if one were to apply the universal local reconstruction concept to the simpler unstructured FD method using nodal unknowns.

In this paper, we introduce a new, high-order, conservative, and efficient method, named the spectral difference (SD) method, for conservation laws on unstructured grids. The method combines the best features of structured and unstructured grid methods to obtain computational efficiency and geometric flexibility. It utilizes the concept of discontinuous and high-order local representations to achieve conservation and high accuracy in a manner similar to the DG and SV methods, but the new method is based on the finite-difference formulation to attain a simpler form and higher efficiency. Specifically, the differential form of the conservation laws is satisfied at nodal unknown points, with flux derivatives expressed in terms of values at flux points.

The paper is organized as follows. In the next section, we first describe the basic formulation of the method. Some representative placements of the unknown and flux points with various orders of accuracy for triangular elements are then presented in Section 3. Accuracy studies of the method are carried out with the two-dimensional linear wave equation and Burgers' equation in Section 4. Each order of accuracy is numerically verified with five unstructured grids of consecutive refinement. Numerical solutions of plane electromagnetic waves incident on perfectly conducting circular cylinders are presented and compared with the exact solutions also in Section 4. Finally, some concluding remarks and suggestions for future study are given in Section 5.

2. The spectral difference method

2.1. General description

The SD method is a type of finite-difference method or nodal spectral method for unstructured grids, in which inside each cell or element we have structured nodal unknown and flux distributions, in such a way that the local integral conservation is satisfied. In considering the SV method, we note that the partitioning of grid cells into subcells is dictated by the need to satisfy the integral conservation law for each cell in order to capture discontinuities. It is then natural to define cell averages of conservative variables as discrete unknowns. But the accuracy of the flux integral for each grid cell is limited by the degree of precision of its reconstruction from the discrete unknowns, and, for non-linear fluxes, the accuracy of the quadrature approximation. Thus the integral unknowns can only be updated with an accuracy of a certain degree of precision. It is therefore sufficient to define the conservative unknowns at quadrature points that will approximate the volume integral over the cell to the desired order of accuracy. The unknowns are updated using the differential form of the conservation law by approximating the flux derivatives at those points. In order to obtain the flux derivatives, we use a polynomial reconstruction of the fluxes from their values at certain flux points. Consequently, we refer to the method as a difference method. Most or all the flux points are located at surface quadrature points that will approximate the flux integral over the grid cell surface to a desired order of accuracy.

In order to minimize the number of unknowns for a given accuracy, the unknowns are normally placed at Gauss quadrature points, while the fluxes are placed at Gauss–Lobatto quadrature points. To evaluate the fluxes, we require the values of unknowns (and their gradients) at flux points. They are obtained from a reconstruction of unknowns using their values at unknown points. The procedure for computing fluxes and their derivatives is similar to that in the pseudo-spectral method, the difference being that the reconstruction of fluxes be one order higher than that of unknowns. On the other hand, in order to avoid an additional reconstruction, one could place both the unknowns and fluxes at the same Gauss–Lobatto quadrature points. However, this would require using more unknowns to achieve a given accuracy. By placing the unknowns and fluxes at the above quadrature points, one can obtain the spectral convergence and accuracy [5,20,22]. Therefore, we also refer to the method as a spectral method.

There are two important features of the method dealing with the relation of the numerical solution in different cells. If the nodes are distributed in a geometrically similar manner for all cells, the discretizations become *universal*, and can be expressed as the same weighted sums of the products of the local metrics and fluxes. These metrics are constants for the line, triangle, and tetrahedron elements, and can be computed analytically for curved elements. In this paper, our formulations are written in general vector forms valid for simplex cells with straight edges and planar faces. Curved elements will be treated in subsequent papers. The other feature concerns the fact that the flux at the surface points between two cells will in general be discontinuous. In order to have local and global conservations, certain flux components must be continuous. We must therefore replace the fluxes at those points with numerical fluxes. The numerical fluxes serve to couple the solutions in two neighboring cells and provide the necessary numerical dissipation to stabilize the numerical method.

2.2. Details of the spectral difference method

The most general form of a conservation law can be written as

$$\frac{\partial u}{\partial t} + \nabla * F = 0, \tag{1}$$

where the conservative variable u can be a scalar or a vector, and the generalized flux F can be a vector or tensor. The term $\nabla * F$ represents the divergence or curl of F ($* \equiv \cdot$ or $\times$), depending on the physical definition of u. The generalized Gauss theorem for a simplex element i can be written as

$$\int_{V_i} \nabla * F \, \mathrm{d}V = \sum_{l=1}^{d+1} \int_{\mathbf{S}_i^l} \mathrm{d}\mathbf{S} * F, \tag{2}$$

where V_i is the volume of element or cell i, and $\mathbf{S}_i^l$ is the area vector of face l for cell i. (In 2D, each face is actually a line.) Here d is the dimension of the domain, and the number of faces for each cell is $d+1$. Integrating (1) over cell i and substituting (2) into (1), we obtain the integral form of the conservation law

$$\frac{\mathrm{d}}{\mathrm{d}t} \int_{V_i} u \, \mathrm{d}V + \sum_{l=1}^{d+1} \int_{\mathbf{S}_i^l} \mathrm{d}\mathbf{S} * F = 0. \tag{3}$$

In order to be consistent with future treatments of curved elements, we now introduce a local coordinate system for each cell. We first choose an origin by assigning the index 0 to an arbitrary vertex and assign the indices $l = 1, d$ to the remaining vertices so as to define a right-handed system. Let $\mathbf{r}_{l,i}$ be the position vector of vertex l of cell i. The set of vectors

$$\mathbf{g}_{l,i} \equiv \mathbf{r}_{l,i} - \mathbf{r}_{0,i}, \quad l = 1, d \tag{4}$$

form a covariant basis defining the local coordinates x^l, as shown in Fig. 1. The position vector $\mathbf{r}$ of any point in cell i is then given by

$$\mathbf{r} = \mathbf{r}_{0,i} + \sum_{l=1}^{d} x^l \mathbf{g}_{l,i}, \quad 0 \leqslant x^l \leqslant 1 \quad \text{and} \quad \sum_{l=1}^{d} x^l \leqslant 1. \tag{5}$$

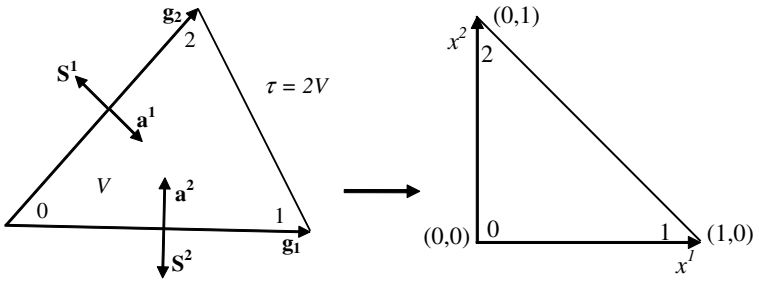

Fig. 1. Transformation of a physical element to the standard element.

In order to obtain a single formulation valid for all dimensions d, we introduce the vector $\mathbf{g}_{2,i}$ as a unit vector normal to $\mathbf{g}_{1,i}$ for $d = 1$, and $\mathbf{g}_{3,i}$ as the unit vector in the direction of $\mathbf{g}_{1,i} \times \mathbf{g}_{2,i}$ for $d = 1$ and 2. We then define

$$\begin{aligned} \mathbf{a}_i^1 &\equiv \mathbf{g}_{2,i} \times \mathbf{g}_{3,i}, \\ \mathbf{a}_i^2 &\equiv \mathbf{g}_{3,i} \times \mathbf{g}_{1,i}, \\ \mathbf{a}_i^3 &\equiv \mathbf{g}_{1,i} \times \mathbf{g}_{2,i} \end{aligned} \tag{6}$$

and

$$\tau_i \equiv \mathbf{g}_{1,i} \cdot \mathbf{g}_{2,i} \times \mathbf{g}_{3,i}. \tag{7}$$

Vectors $\mathbf{a}_i^l$, $l = 1, d$, form another set of basis vectors with $\mathbf{a}_i^l/\tau_i (= \mathbf{g}_i^l)$ being the contravariant basis vector of $\mathbf{g}_{l,i}$. Geometrically, $\mathbf{a}_i^l$ and τ_i are related to the surface areas $\mathbf{S}_i^l$ and cell volume V_i of the cell (simplex with straight edges and planar faces) by

$$\mathbf{a}_i^l = -((d-1)!)\mathbf{S}_i^l \tag{8}$$

and

$$\tau_i = (d!)V_i. \tag{9}$$

Since $\nabla \equiv \sum_{l=1}^{d} \mathbf{g}_i^l \frac{\partial}{\partial x^l}$, we now can write $\nabla * F$ in each cell in terms of the local coordinates x^l and the basis vectors $\mathbf{a}_i^l$ as

$$\nabla * F = \frac{1}{\tau_i} \sum_{l=1}^{d} \mathbf{a}_i^l * \frac{\partial F}{\partial x^l}, \tag{10a}$$

or in the conservative form

$$\nabla * F = \frac{1}{\tau_i} \sum_{l=1}^{d} \frac{\partial (\mathbf{a}_i^l * F)}{\partial x^l}. \tag{10b}$$

The form (10b) is necessary when treating curved elements. We will seek finite-difference approximations to Eqs. (10) in terms of metric and flux values at flux points. Here, instead of adopting the conventional multi-dimensional Taylor series expansion approach, we will employ a more general approach using reconstruction. Although both approaches result in the same difference operators for non-singular systems, the latter is capable of handling over-specified systems.

In each cell, the discrete unknowns are the values of u at quadrature points for the volume integral over the cell. We denote these points, some of which may lie on the cell faces, as $\mathbf{r}_{j,i}$, and define

$$u_{j,i} \equiv u_i(\mathbf{r}_{j,i}). \tag{11}$$

We also denote by $\mathbf{x}$ the local position vector in the transformed "Cartesian" space defined by the coordinates x^l. If the points $\mathbf{r}_{j,i}$ are distributed in a geometrically similar manner for all cells, they all have the same local position $\mathbf{x}_j$. Therefore, we can rewrite Eq. (11) as

$$u_{j,i} = u_i(\mathbf{x}_j). \tag{12}$$

In order to reconstruct u within each cell, we introduce a set of complete polynomials $\phi_n(\mathbf{x})$ of degree p and expand $u_i(\mathbf{x})$ in the ith cell as

$$u_i(\mathbf{x}) = \sum_{n=1}^{N_p^d} c_{n,i} \phi_n(\mathbf{x}). \tag{13}$$

Here

$$N_p^d = \frac{(p+d)!}{p!d!} = \begin{cases} (p+1) & d = 1, \\ (p+1)(p+2)/2 & d = 2, \\ (p+1)(p+2)(p+3)/6 & d = 3. \end{cases} \tag{14}$$

Eq. (12) can then be written as

$$u_{j,i} = \sum_{n=1}^{N_p^d} R_{jn} c_{n,i}, \tag{15}$$

where

$$R_{jn} = \phi_n(\mathbf{x}_j). \tag{16}$$

One requires N_p^d point values in each cell i to reconstruct a degree p polynomial if the resulting reconstruction matrix R_{jn} is non-singular. The elimination of the coefficients $c_{n,i}$ in Eq. (15) can be shown succinctly using matrix algebra. Let c_i, u_i, and $\phi(\mathbf{x})$ be algebraic vectors with components $c_{n,i}$, $u_{j,i}$, and $\phi_n(\mathbf{x})$, respectively, and let R be the matrix with elements R_{jn}. Eqs. (13) and (15) can then be written as

$$u_i(\mathbf{x}) = \phi^{\mathrm{T}}(\mathbf{x})\mathsf{c}_i \tag{17}$$

and

$$\mathsf{u}_i = \mathsf{R}\mathsf{c}_i. \tag{18}$$

Since $\mathbf{x}_j$ are the same for all cells and therefore so is R, it is now clear that the reconstruction becomes universal. Eliminating c_i, we obtain

$$u_i(\mathbf{x}) = \mathsf{L}(\mathbf{x})\mathsf{u}_i, \tag{19}$$

where

$$\mathsf{L}(\mathbf{x}) \equiv \phi^{\mathrm{T}}(\mathbf{x})\mathsf{R}^{-1}. \tag{20}$$

In order to evaluate the surface integrals in (3) efficiently, we discretize F at points $\mathbf{r}_{k,i}$, most or all of which are located at quadrature points for those integrals. Since the flux derivatives are used to update the conservative unknowns, the flux points should support a polynomial reconstruction of degree $p+1$. A similar procedure is used for the reconstruction of F. As in the case for the unknown points $\mathbf{r}_{j,i}$, if the flux points $\mathbf{r}_{k,i}$ are distributed in a geometrically similar manner for all cells, they all also have the same local position $\mathbf{x}_k$. This also leads to a universal reconstruction for F.

There are possible circumstances in which the reconstruction matrix for u or F is singular. In such a case, we can choose a different set of points or simply add additional points, generally one point at the centroid of the cell, to remove the singularity. For the latter, we then use a least-squares method, the same one used in the UFV method, for the reconstruction. All the equations above are still valid, except R^{-1} is now replaced by the pseudo-inverse R^{+}. Although the matrix R can be ill-conditioned, we use *Mathematica* [44] to obtain its inverse or pseudo-inverse analytically.

Let N_u be the number of unknown points in each cell. Eq. (19) can then be written in an expanded form

$$u_i(\mathbf{x}) = \sum_{j=1}^{N_u} L_j(\mathbf{x}) u_{j,i}. \tag{21}$$

Here the functions $L_j(\mathbf{x})$, which are the components of the algebraic row vector $L(\mathbf{x})$, are known as shape functions. The locations of $\mathbf{x}_j$ then uniquely define the basis $L_j(\mathbf{x})$. Similarly, let N_F be the number of flux points in the cell and define

$$F_{k,i} \equiv F_i(\mathbf{r}_{k,i}) = F_i(\mathbf{x}_k), \tag{22}$$

the expansion of F can also be written as

$$F_i(\mathbf{x}) = \sum_{k=1}^{N_F} M_k(\mathbf{x}) F_{k,i}. \tag{23}$$

Here $M_k(\mathbf{x})$ are now the set of shape functions defined by the $\mathbf{x}_k$. Using Eq. (10), we can satisfy (1) at points $\mathbf{r}_{j,i}$ by evaluating

$$\nabla * F(\mathbf{r}_{j,i}) = \frac{1}{\tau_i} \sum_{l=1}^{d} \mathbf{a}_i^l * \sum_{k=1}^{N_F} m_{jk,l} F_{k,i} \tag{24a}$$

or

$$\nabla * F(\mathbf{r}_{j,i}) = \frac{1}{\tau_i} \sum_{l=1}^{d} \sum_{k=1}^{N_F} m_{jk,l} \mathbf{a}_i^l * F_{k,i}, \tag{24b}$$

whichever is more efficient. The coefficients

$$m_{jk,l} = \frac{\partial M_k(\mathbf{x}_j)}{\partial x^l} \tag{25}$$

are universal constants. In order to evaluate $F_{k,i}$, $u_{k,i}$ is required, which can be obtained directly from (21) as

$$u_{k,i} = \sum_{j=1}^{N_u} l_{kj} u_{j,i}, \tag{26}$$

where

$$l_{kj} = L_j(\mathbf{x}_k) \tag{27}$$

are also universal constants. To reduce the cost of interpolation (26), some of the points $\mathbf{r}_{k,i}$ may be chosen to coincide with $\mathbf{r}_{j,i}$. There are only a few of these coefficients in (25) and (27), which can be calculated exactly and stored in advance.

For those points $\mathbf{r}_{k,i}$ located on the cell faces, since u may be discontinuous, the fluxes at those points are not uniquely defined. As a result, we must replace the fluxes with "numerical fluxes", which can be computed using exact or approximate Riemann solvers, e.g. [33,34]. These numerical fluxes are responsible for coupling the solutions in two adjoining cells and providing the necessary numerical dissipation to stabilize the numerical method. Note that in a finite volume method, only the normal component ($\mathbf{n} \cdot F$) or the tangential component ($\mathbf{n} \times F$) of the flux is used in the formulation. In the SD method, the full flux vectors at all the flux points are necessary to update the solution unknowns. However, to satisfy local conservation, the same normal or tangential components must be used on the two cells sharing a common face. In order to describe how the numerical fluxes are computed, refer to Fig. 2, in which flux points are further classified as corner points or face points. If the underlying physics of the conservation laws is a simple uni-directional wave in the direction $\boldsymbol{l}$, an "exact" multi-dimensional Riemann solver can be used to determine the common flux independent of the computational mesh. For example, for both the corner and face points, we need to first identify the cell where the wave is coming from. For the face point shown in Fig. 2, the cell is D, and for the corner point, the cell is A. Then the numerical flux vector at the face or corner points are replaced with the flux vector computed based on the interpolated state variable from the identified cell, i.e., cell D for the face point and face A for the corner

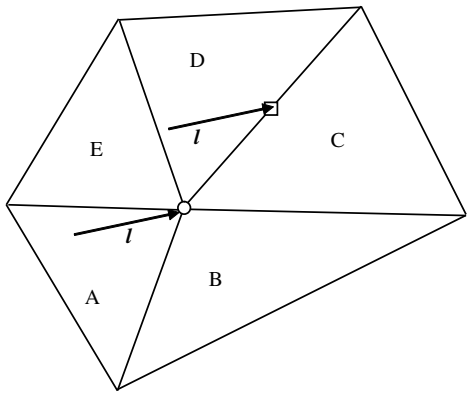

Fig. 2. Flux computation for a corner (○) and a face (□) point using a multi-dimensional Riemann solver.

point. For complex systems of conservation laws, it may be impossible to decompose the physics into that of simple waves. In such cases, approximate Riemann solvers are employed to compute the numerical flux. Consider cell C in Fig. 3. For the face flux point, the outgoing face normal is $\boldsymbol{n}_1$. In the case of divergence ($* = \cdot$), the normal component of the flux vector can be computed with any 1D Riemann solver. However, we have the complete freedom in how to determine the tangential component of the flux vector at the face point since it does not affect the conservation property. In fact, it is not strictly necessary to have a unique tangential component physically at the face point (e.g. a contact discontinuity in which density is discontinuous). Here we offer two choices. One is to use a common tangential component by averaging the two tangential components from both sides of the face. The other choice is to use its own tangential component from the current cell, allowing the tangential component to be discontinuous. For the corner point, two normals ($\boldsymbol{n}_1, \boldsymbol{n}_2$) can be defined, i.e., $\boldsymbol{n}_1$ pointing from cell C to cell *1* and $\boldsymbol{n}_2$ from cell C to cell 2. Two 1D Riemann solvers are then used to compute the fluxes in $\boldsymbol{n}_1$ and $\boldsymbol{n}_2$ directions, F_{n_1} and F_{n_2}. The full flux vector can be solved directly from F_{n_1} and F_{n_2}. Similar procedures can be used for the case of curl ($* = \times$), in which the tangential components of the flux vectors are computed with a 1D Riemann solver.

Quadrature approximations to integrals over simplexes of various degrees of precision can be obtained using Table 1 of [27]. If one chooses unknown locations $\mathbf{r}_{j,i}$ and corresponding weights that yield an approximation of degree of precision of at least p for the volume integral, and flux locations $\mathbf{r}_{k,i}$ and corresponding weights that yield an approximation of degree of precision of at least $p+1$, then the integral conservation (3) will be satisfied locally to the order of accuracy of the method. One can also choose the locations $\mathbf{r}_{j,i}$ and $\mathbf{r}_{k,i}$ to yield quadrature approximations of even higher degrees of precision. We can further place $\mathbf{r}_{j,i}$ and $\mathbf{r}_{k,i}$ such that the local integral conservation (3) is exactly satisfied *numerically*. Using a quadrature approximation, the volume integral can be written as

$$\int_{V_i} \nabla * F \, \mathrm{d}V = V_i \sum_{j}^{N_u} w_j \nabla * F(\mathbf{r}_{j,i}). \tag{28a}$$

Here w_j are the volume quadrature weights at the points $\mathbf{r}_{j,i}$. Substituting (8), (9), and (24) into the above equation, one obtains

$$\int_{V_i} \nabla * F \, \mathrm{d}V_i = -\frac{1}{d!} \sum_{l=1}^{d} \sum_{k=1}^{N_F} \sum_{j=1}^{N_u} w_j m_{jk,l} \mathbf{S}_i^l * F_{k,i}. \tag{28b}$$

Similarly, the surface integral of F can be expressed as

$$\sum_{l=1}^{d+1} \int_{\mathbf{S}_i^l} \mathrm{d}\mathbf{S} * F = \sum_{l=1}^{d+1} \sum_{k} w_k \mathbf{S}_i^l * F_{k,i}. \tag{29}$$

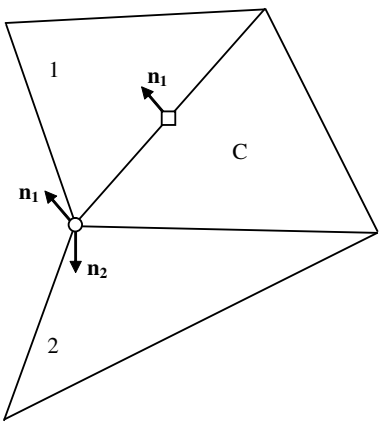

Fig. 3. Flux computation for a corner (○) and a face (□) point using a one-dimensional Riemann solver.

Here w_k are surface quadrature weights for face l, and for each face the summation is over those points $\mathbf{r}_{k,i}$ located on that face. In order that the local integral conservation (3) is exactly satisfied numerically, Eq. (28b) and the resulting equation of (29) using the relation $\sum_{l=1}^{d+1}\mathbf{S}_i^l = 0$ must have the same coefficient for each $F_{k,i}$. In particular, the total contribution from any interior point $F_{k,i}$ to the volume integral in (28) must vanish.

The SD formulation for the line element is similar to the multidomain spectral method. Here the distributions of u and F points are based on those quadrature points that lead to the satisfaction of the integral form of the conservation law. Since this does not define a unique set of locations, they can be optimized by minimizing some object functions. The tensor products of the line formulation can be used for quadrilateral and hexahedral cells or elements.

From (24) and (26), we also see that the SD formulation is very similar to that of the FD method for structured grids. The SD method thus retains the simplicity and computational efficiency of the structured FD method. However, the metric terms in the latter are evaluated by numerically differencing the grid point coordinates. Since numerical grid generators are mostly only second-order accurate, the overall accuracy of the solution can be severely degraded if the grid is not sufficiently smooth. In contrast, the metric terms in the SD method are computed exactly from the geometry of the grid, no matter how it was generated. It thus retains its formal accuracy, even for very unsmooth unstructured grids. Furthermore, in contrast to the FD method, the integral conservation law is satisfied to the desired accuracy. In the remainder of the paper, we limit ourselves to triangular grids. Tetrahedral grids will be treated in subsequent papers.

3. Locations of the unknown and flux points for triangles

3.1. General criteria

The critical part of the SD method is the location of the u points $\mathbf{r}_{j,i}$ and F points $\mathbf{r}_{k,i}$. If those points are distributed in a geometrically similar manner for all cells, the formulas for the flux derivatives become universal, and can be expressed as the same weighted sums of the products of the local metrics and fluxes. The locations of the u and F points are determined by symmetry groups associated with the cell centroid, vertices, and edges. All but the first contain arbitrary parameters that can be varied to obtain optimum solutions. The number of points required for a reconstruction with a specified degree of precision is greater than the minimum number of Gaussian quadrature points for that precision. One can obtain greater efficiency by locating some u points on the cell boundary, to coincide with F points, and utilizing a Gauss–Lobatto quadrature formula. For F points on the vertices (2D and 3D) and edges (3D), more than one Riemann solver is necessary. For those formulations with expensive Riemann solvers, these points should be minimized. Another criterion for the placement of u or F points is that the reconstruction matrix should be non-singular if possible. If additional points are needed, the rank of the reconstruction matrix must be the same as the number of basis functions used. Even in this case, we can show that the number of F points is far less than the number of flux quadrature points in the SV method with the same accuracy. The final criterion is that integral conservation is satisfied within the desired degree of precision.

3.2. Symmetry groups

We first describe symmetry groups for a triangle, as discussed in [27]. While in Section 2 subscripts were used as generic indices for cells and u and F points, in this section they will indicate vertices and edges for a given triangle. A single subscript will refer to a vertex, while a double subscript will refer to an edge. The symmetry is most clearly evident when viewed from the centroid of the triangle. We will therefore find it useful to characterize the symmetry groups in terms of parameterizations based on the centroid.

Let $\mathbf{r}_m$ be the position vector of vertex m. Then its position vector with respect to the centroid is defined as

$$\bar{\mathbf{r}}_m \equiv \mathbf{r}_m - \mathbf{r}^c, \tag{30}$$

where the centroid $\mathbf{r}^c$ is given as

$$\mathbf{r}^{c} = \frac{1}{3}\sum_{m} \mathbf{r}_m. \tag{31}$$

The first symmetry group consists of the centroid $\mathbf{r}^{c}$. This group is necessary when the total number of points supporting a polynomial is not divisible by 3. The second symmetry group consists of the three one-parameter vertex-based points

$$\bar{\mathbf{r}}_m^{\alpha} \equiv \alpha \bar{\mathbf{r}}_m \quad \left(-\frac{1}{2} \leqslant \alpha \leqslant 1, \alpha \neq 0\right). \tag{32}$$

$\alpha = 1$ corresponds to the vertex, while $\alpha = -1/2$ is the midpoint of the opposite edge. $\alpha = 0$ corresponds to the centroid, and therefore must be excluded from this symmetry group. The third symmetry group consists of the six two-parameter edge-based points

$$\bar{\mathbf{r}}_{mn}^{\gamma\delta} \equiv \gamma \bar{\mathbf{r}}_m + \delta \bar{\mathbf{r}}_n \quad (m \neq n, \gamma \neq \delta \neq 0) \tag{33}$$

for edge mn connecting vertices m and n. To exclude points which are already in the first two groups, γ and δ must not equal zero, and m must not equal n. We must also exclude the special case $\gamma = \delta$, since this is already covered by the vertex-based group. It is easy to show that the values of γ and δ in the $\gamma - \delta$ plane are restricted to the triangle determined by the points $(0,1)$, $(1,0)$, and $(-1,-1)$ in order for the points to lie within the triangle. When $\gamma + \delta = 1$, the points lie on the edge mn. This special group plays an important role in the locations of the F points, which are found primarily on the edges of the triangle.

3.3. Representative placements of u and F points

Eq. (14) gives the minimum number of points required in a reconstruction that supports a polynomial of degree p. If the u points support a polynomial of degree p, the F points should support a polynomial of degree $p+1$, and the order of accuracy of the method is $p+1$. While the accuracy of the SD method depends on the locations of u and F, here we present only some representative placements of u and F points that satisfy the integral conservation law, for various orders of accuracy. These placements do not necessarily represent the best choices, but they do show the orders of accuracy as claimed in our numerical tests. The placements of the points are shown geometrically in Fig. 4, with u in circles and F in squares. The corresponding vectors $\mathbf{g}_l$, $\mathbf{a}^l$, and $\mathbf{S}^l$ (not scaled), and scalars V and τ are depicted in Fig. 1. Numerical values for the coefficients l_{kj} and $m_{jk,l}$ are presented for some first and second-order accuracy placements. Due to space limitation, the values for other placements can be obtained by contacting the first author. The optimization of the locations will be studied in the future.

3.3.1. First-order accuracy

From (14) it follows that we need one u point and three F points. The u point is at the centroid (volume quadrature weight $w = 1$). There are two possibilities for the F points. They can be located at the edge midpoints ($\alpha = -\frac{1}{2}$, and surface quadrature weight $w = 1$) defining placement 1a shown in Fig. 4a, or at the vertices ($\alpha = 1,\ w = \frac{1}{2}$), defining placement 1b shown in Fig. 4b. For a piecewise constant reconstruction, the u at any point is simply the u at the centroid, and thus for both the placements

$$\begin{bmatrix} u_1 \\ u_2 \\ u_3 \end{bmatrix} = u_a. \tag{34}$$

We can also show that

$$[\nabla * F_a]\tau = [2 \quad -2 \quad 0] \begin{bmatrix} \mathbf{a}^1 * F_1 \\ \mathbf{a}^1 * F_2 \\ \mathbf{a}^1 * F_3 \end{bmatrix} + [2 \quad 0 \quad -2] \begin{bmatrix} \mathbf{a}^2 * F_1 \\ \mathbf{a}^2 * F_2 \\ \mathbf{a}^2 * F_3 \end{bmatrix} \tag{35a}$$

for the placement 1a, and

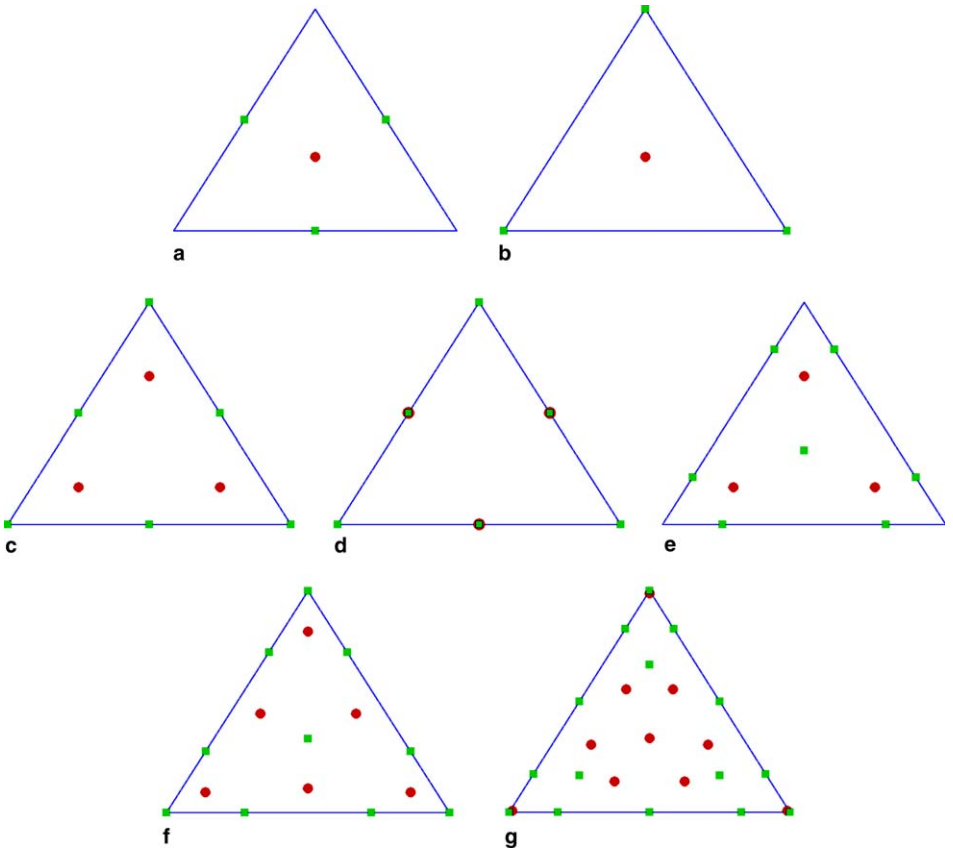

Fig. 4. Placement of unknown (●) and flux (■) points for a triangular element. First order: (a)–(b); second order: (c)–(e); third order: (f); fourth order: (g).

$$[\nabla * F_a]\tau = [-1 \quad 1 \quad 0]\begin{bmatrix} \mathbf{a}^1 * F_1 \\ \mathbf{a}^1 * F_2 \\ \mathbf{a}^1 * F_3 \end{bmatrix} + [-1 \quad 0 \quad 1]\begin{bmatrix} \mathbf{a}^2 * F_1 \\ \mathbf{a}^2 * F_2 \\ \mathbf{a}^2 * F_3 \end{bmatrix} \tag{35b}$$

for the placement 1b. Using Eqs. (35) and the corresponding volume and surface quadrature weights, one can easily verify that Eqs. (28) and (29) yield the same form and thus the local integral conservation is exactly satisfied numerically. In addition, one can show that Eqs. (35) also satisfy the geometrical conservation by assuming a uniform F field. Since u is a constant inside each cell, except at boundaries, both placements actually produce the same solution. Furthermore, for the first-order accuracy, the UFV, DG, SV, and SD methods all yield exactly the same formulation.

3.3.2. Second-order accuracy

For the second-order accuracy, we now need three u points and six F points. We can place all six F points on the edges to obtain higher accurate surface quadrature approximations. The first choice involves two vertex-based symmetry groups, three points at the vertices ($\alpha = 1,\ w = \frac{1}{6}$), and three points at the edge midpoints ($\alpha = -\frac{1}{2},\ w = \frac{4}{6}$). The surface quadrature approximation for this placement corresponds to the fourth-order Simpson rule. The three u points involve one vertex-based group. There are two Gaussian placements, both giving third-order accuracy for the volume quadrature formula. In placement 2a, shown in Fig. 4c, the u points are given by ($\alpha = \frac{1}{2},\ w = \frac{1}{3}$), and in placement 2b, shown in Fig. 4d, the u points are at the edge midpoints ($\alpha = -\frac{1}{2},\ w = \frac{1}{3}$). Note that in placement 2b the u points coincide with 3 of the F points, reducing the number of interpolations. For the placement 2a,

$$\begin{bmatrix} u_1 \\ u_2 \\ u_3 \\ u_4 \\ u_5 \\ u_6 \end{bmatrix} = \begin{bmatrix} -\frac{1}{3} & \frac{5}{3} & -\frac{1}{3} \\ -\frac{1}{3} & \frac{2}{3} & \frac{2}{3} \\ -\frac{1}{3} & -\frac{1}{3} & \frac{5}{3} \\ \frac{2}{3} & -\frac{1}{3} & \frac{2}{3} \\ \frac{5}{3} & -\frac{1}{3} & -\frac{1}{3} \\ \frac{2}{3} & \frac{2}{3} & -\frac{1}{3} \end{bmatrix} \begin{bmatrix} u_a \\ u_b \\ u_c \end{bmatrix} \tag{36a}$$

and

$$\begin{bmatrix} \nabla * F_a \\ \nabla * F_b \\ \nabla * F_c \end{bmatrix} \tau = \begin{bmatrix} -\frac{1}{3} & \frac{2}{3} & 0 & -\frac{2}{3} & -\frac{5}{3} & 2 \\ \frac{5}{3} & \frac{2}{3} & 0 & -\frac{2}{3} & \frac{1}{3} & -2 \\ -\frac{1}{3} & \frac{8}{3} & 0 & -\frac{8}{3} & \frac{1}{3} & 0 \end{bmatrix} \begin{bmatrix} \mathbf{a}^1 * F_1 \\ \mathbf{a}^1 * F_2 \\ \mathbf{a}^1 * F_3 \\ \mathbf{a}^1 * F_4 \\ \mathbf{a}^1 * F_5 \\ \mathbf{a}^1 * F_6 \end{bmatrix} + \begin{bmatrix} 0 & \frac{2}{3} & -\frac{1}{3} & 2 & -\frac{5}{3} & -\frac{2}{3} \\ 0 & \frac{8}{3} & -\frac{1}{3} & 0 & \frac{1}{3} & -\frac{8}{3} \\ 0 & \frac{2}{3} & \frac{5}{3} & -2 & \frac{1}{3} & -\frac{2}{3} \end{bmatrix} \begin{bmatrix} \mathbf{a}^2 * F_1 \\ \mathbf{a}^2 * F_2 \\ \mathbf{a}^2 * F_3 \\ \mathbf{a}^2 * F_4 \\ \mathbf{a}^2 * F_5 \\ \mathbf{a}^2 * F_6 \end{bmatrix} \tag{36b}$$

and for the placement 2b,

$$\begin{bmatrix} u_1 \\ u_2 \\ u_3 \\ u_4 \\ u_5 \\ u_6 \end{bmatrix} = \begin{bmatrix} 1 & -1 & 1 \\ 1 & 0 & 0 \\ 1 & 1 & -1 \\ 0 & 1 & 0 \\ -1 & 1 & 1 \\ 0 & 0 & 1 \end{bmatrix} \begin{bmatrix} u_a \\ u_b \\ u_c \end{bmatrix} \tag{37a}$$

and

$$\begin{bmatrix} \nabla * F_a \\ \nabla * F_b \\ \nabla * F_c \end{bmatrix} \tau = \begin{bmatrix} 1 & 2 & 0 & -2 & 1 & -2 \\ -1 & 2 & 0 & -2 & -1 & 2 \\ 1 & 0 & 0 & 0 & -1 & 0 \end{bmatrix} \begin{bmatrix} \mathbf{a}^1 * F_1 \\ \mathbf{a}^1 * F_2 \\ \mathbf{a}^1 * F_3 \\ \mathbf{a}^1 * F_4 \\ \mathbf{a}^1 * F_5 \\ \mathbf{a}^1 * F_6 \end{bmatrix} + \begin{bmatrix} 0 & 2 & 1 & -2 & 1 & -2 \\ 0 & 0 & 1 & 0 & -1 & 0 \\ 0 & 2 & -1 & 2 & -1 & -2 \end{bmatrix} \begin{bmatrix} \mathbf{a}^2 * F_1 \\ \mathbf{a}^2 * F_2 \\ \mathbf{a}^2 * F_3 \\ \mathbf{a}^2 * F_4 \\ \mathbf{a}^2 * F_5 \\ \mathbf{a}^2 * F_6 \end{bmatrix}. \tag{37b}$$

If we move the F points to the Gaussian points on the edges $\left(\gamma = \frac{3+\sqrt{3}}{6},\ \delta = \frac{3-\sqrt{3}}{6},\ w = \frac{1}{2}\right)$ in order to minimize the Riemann solver calls, the result is a singular matrix. The singularity can be removed by adding an F point at the centroid, and this defines the placement 2c as shown in Fig. 4e. This placement requires a least-squares inversion to obtain a reconstruction for F. Again, all three placements satisfy the local integral conservation and geometrical conservation.

3.3.3. Third-order accuracy

We now need 6 u points and 10 F points. The u points can consist of one edge-based symmetry group or two vertex-based symmetry groups. However, the former would be singular and the latter are just sufficient for a fifth-order Gaussian volume quadrature formula if we choose $\alpha_1 = \frac{-10+5\sqrt{10}+\sqrt{950-220\sqrt{10}}}{30}$ and $\alpha_2 = \frac{-10+5\sqrt{10}-\sqrt{950-220\sqrt{10}}}{30}$. The corresponding weights are $w_1 = \frac{5\alpha_2-2}{60\alpha_1^2(\alpha_2-\alpha_1)}$ and $w_2 = \frac{5\alpha_1-2}{60\alpha_2^2(\alpha_1-\alpha_2)}$. The F distribution requires a point at the centroid. The remaining 9 points can be most efficiently distributed at Gauss–Lobatto points on the edges, involving one vertex-based group ($\alpha = 1,\ w = \frac{1}{12}$), and one edge-based group ($\gamma = \frac{5+\sqrt{5}}{10},\ \delta = \frac{5-\sqrt{5}}{10},\ w = \frac{5}{12}$). The resulting placements are shown in Fig. 4f.

3.3.4. Fourth-order accuracy

We need 10 u points and 15 F points. One u point is located at the centroid. The remaining 9 points can be satisfied by three vertex-based groups. Unfortunately this results in a singular matrix. We therefore need one edge-based group and one vertex-based group for the u points. In our initial study, $(\gamma = \frac{5}{12},\ \delta = \frac{1}{6})$ were used for the edge-based group, and $(\alpha = \frac{3367+\sqrt{14205289}}{7584})$ was used for the vertex-based group. These parameters were derived from Table 1 of [27] for a fifth-order volume quadrature. The 15 F points could all be located on the edges of the triangle, but this again results in a singular matrix. We therefore need at least one symmetry group for F whose points lie in the interior. Here we arbitrarily chose one vertex-based group with $(\alpha = \frac{1}{2})$. Again, the remaining 12 points can be most efficiently distributed at Gauss–Lobatto points on the edges, involving two vertex-based groups $(\alpha = 1)$ and $(\alpha = -\frac{1}{2})$, and one edge-based group $(\gamma = \frac{7+\sqrt{21}}{14},\ \delta = \frac{7-\sqrt{21}}{14})$. The resulting placements are shown in Fig. 4g. We would like to emphasize that this initial choice is by no means an optimum choice. Nevertheless, it does show a fourth-order accuracy in our numerical tests.

4. Numerical results

4.1. Accuracy study with 2D linear wave equation

We first test the accuracy of the SD method on the two-dimensional linear wave equation

$$\begin{aligned} &\frac{\partial u}{\partial t} + \frac{\partial u}{\partial x} + \frac{\partial u}{\partial y} = 0, \quad -1 \leqslant x \leqslant 1,\ -1 \leqslant y \leqslant 1, \\ &u(x, y, 0) = \sin \pi(x + y), \quad \text{periodic boundary condition.} \end{aligned} \tag{38}$$

A $10 \times 10 \times 2$ unstructured grid over the square domain $(-1 \leqslant x \leqslant 1, -1 \leqslant y \leqslant 1)$ is shown in Fig. 5. Note that the cells in the irregular grid have quite different sizes. Five grids of successive refinement were used in the study. The finer grids were generated recursively by cutting each coarser grid cell into four finer grid cells. The boundary fluxes on each triangular element's face were computed using the multi-dimensional Riemann solver, since this is an exact Riemann solver for the wave equation. This solution is then updated at each time step using a third-order TVD Runge–Kutta scheme [35]. The numerical simulation was carried until $t = 1$. In Fig. 6a, we plot the L_1 and L_∞ error norms using the first to fourth-order SD schemes with the u and F placements given in Figs. 4a, and c, f, and g, respectively. The errors presented in the figure are time step independent because the time step Δt was made small enough so that the errors are dominated by the spatial discretization. It is easily verified from the figure that all schemes are convergent with grid refinement and the expected orders of accuracy have been achieved. In Fig. 6b, we show the same error norms using the second to fourth order SV schemes [41]. It is shown that the SD method has similar errors as the SV method in this test. The SD method is over twice as fast as the SV method for this case.

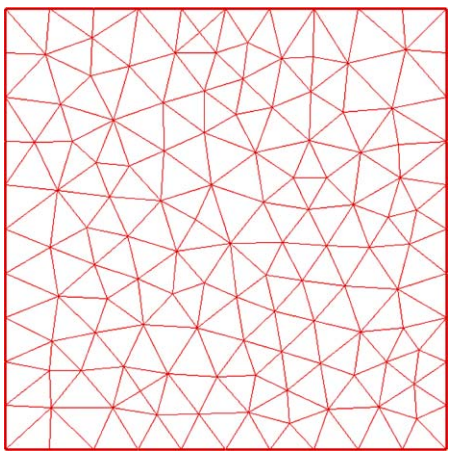

Fig. 5. An unstructured grid over a square domain.

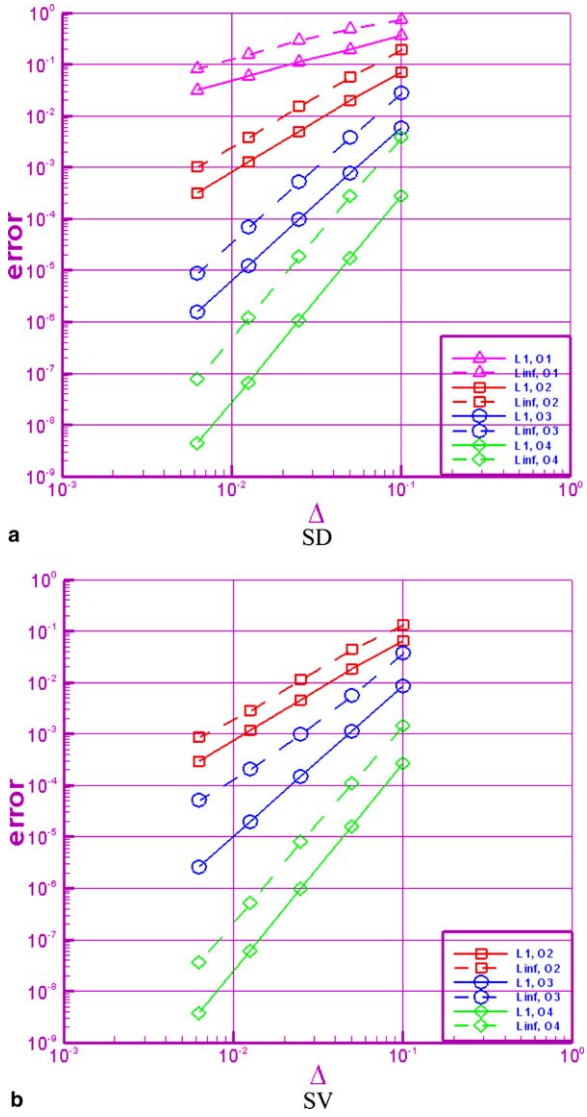

Fig. 6. Error norms of various order of accuracy for the 2D linear wave equation at $t = 1.0$.

4.2. Burgers' equation and shock capturing

In this case, we test the accuracy of the SD method on the two-dimensional Burgers' equation:

$$\begin{aligned} &\frac{\partial u}{\partial t} + \frac{\partial u^2/2}{\partial x} + \frac{\partial u^2/2}{\partial y} = 0, \quad -1 \leqslant x \leqslant 1, \quad -1 \leqslant y \leqslant 1, \\ &u(x, y, 0) = \frac{1}{4} + \frac{1}{2}\sin \pi(x + y), \text{ periodic boundary condition.} \end{aligned} \tag{39}$$

The test was carried out using the same first to fourth-order SD schemes and the same time integration scheme on the same grids as used in the previous test. The boundary fluxes on each element's face were first computed with the multi-dimensional Riemann solver. We started with a smooth initial solution. Due to the non-linearity of the Burgers equation, discontinuities will develop in the solution. At $t = 0.1$, the exact solution is still smooth. The numerical simulation was therefore carried out until $t = 0.1$ without the use of limiters. In Fig. 7a, we present the L_1 and L_∞ errors of the four SD schemes. All schemes are convergent with grid refinement and the

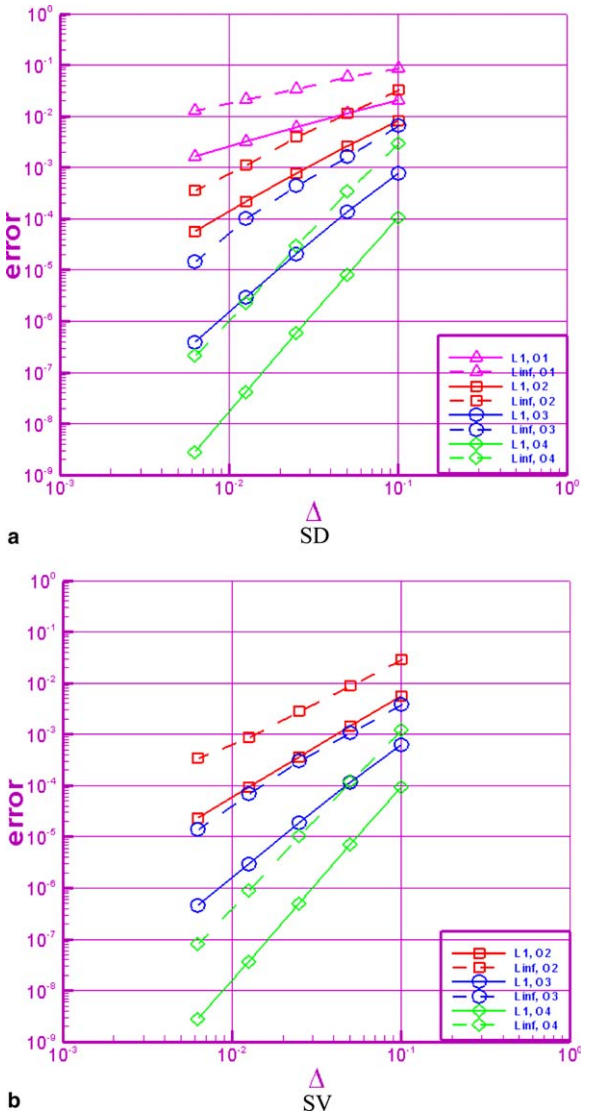

Fig. 7. Error norms of various order of accuracy for the 2D Burgers' equation at $t = 0.1$.

expected orders of accuracy have been achieved, although there is a slight loss of accuracy in the L_∞ norm, probably due to the non-linear nature of the Burgers equation. In Fig. 7b, we also show the same error norms using the second to fourth-order SV schemes [41]. Again, the SD method has similar errors as the SV method in this test. We then carried out the test with a different way to compute the boundary fluxes using the one-dimensional Rusanov or Roe Riemann solver [33,34]. The errors are similar to the previous test with fully upwind fluxes. At $t = 0.45$, the exact solution has developed two shock waves, and limiters were then used to handle the discontinuities. A TVD limiter implemented here is very similar to that for the SV method [41]. The basic idea of limiter can be described in the following steps:

- Compute the cell averaged state variable $\bar{u}_i$ for each cell using the volume quadrature rule.
- For each cell, compute the minimum and maximum mean solutions $\bar{u}_i^{\min}$, $\bar{u}_i^{\max}$ from neighboring cells sharing a node.
- If the reconstructed solution at any of the flux points falls out of the range $[\bar{u}_i^{\min}, \bar{u}_i^{\max}]$, the solution is assumed linear with the following distribution

$$u_i(\mathbf{r}) = \bar{u}_i + \varphi_i \nabla u_i \cdot (\mathbf{r} - \mathbf{r}_c), \tag{40}$$

where ∇u_i is the gradient computed at the cell centroid based on the original reconstruction, φ_i is a scalar limiter in $[0,1]$. The limiter is so chosen that the solutions at all flux points are within the range $[\bar{u}_i^{\min}, \bar{u}_i^{\max}]$. This limiter is applied after each solution update.

Shown in Fig. 8 are the exact solution and the numerical solutions with the second, third, and fourth-order SD schemes using the multi-dimensional Riemann solver on the $40 \times 40 \times 2$ irregular grid. The shock waves are captured well in all cases.

4.3. Scattering of an electromagnetic plane wave incident on a perfectly conducting cylinder

In order to demonstrate the high accuracy of the method, it was decided in this initial phase to choose problems for which there exist exact solutions. To this end we solve the Maxwell equations

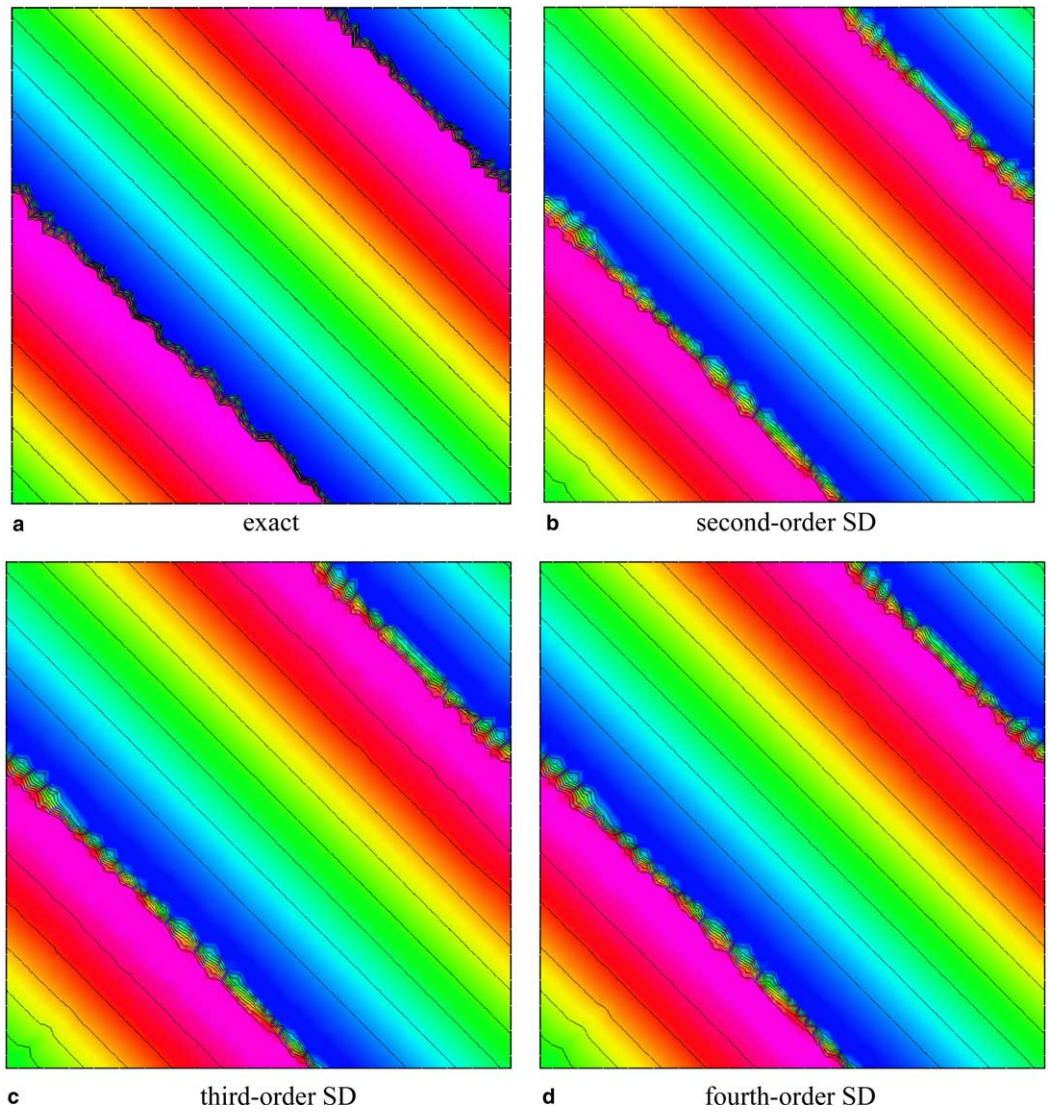

Fig. 8. Solutions of 2D Burgers' equation at $t = 0.45$ (10 contours between -0.25 and 0.75).

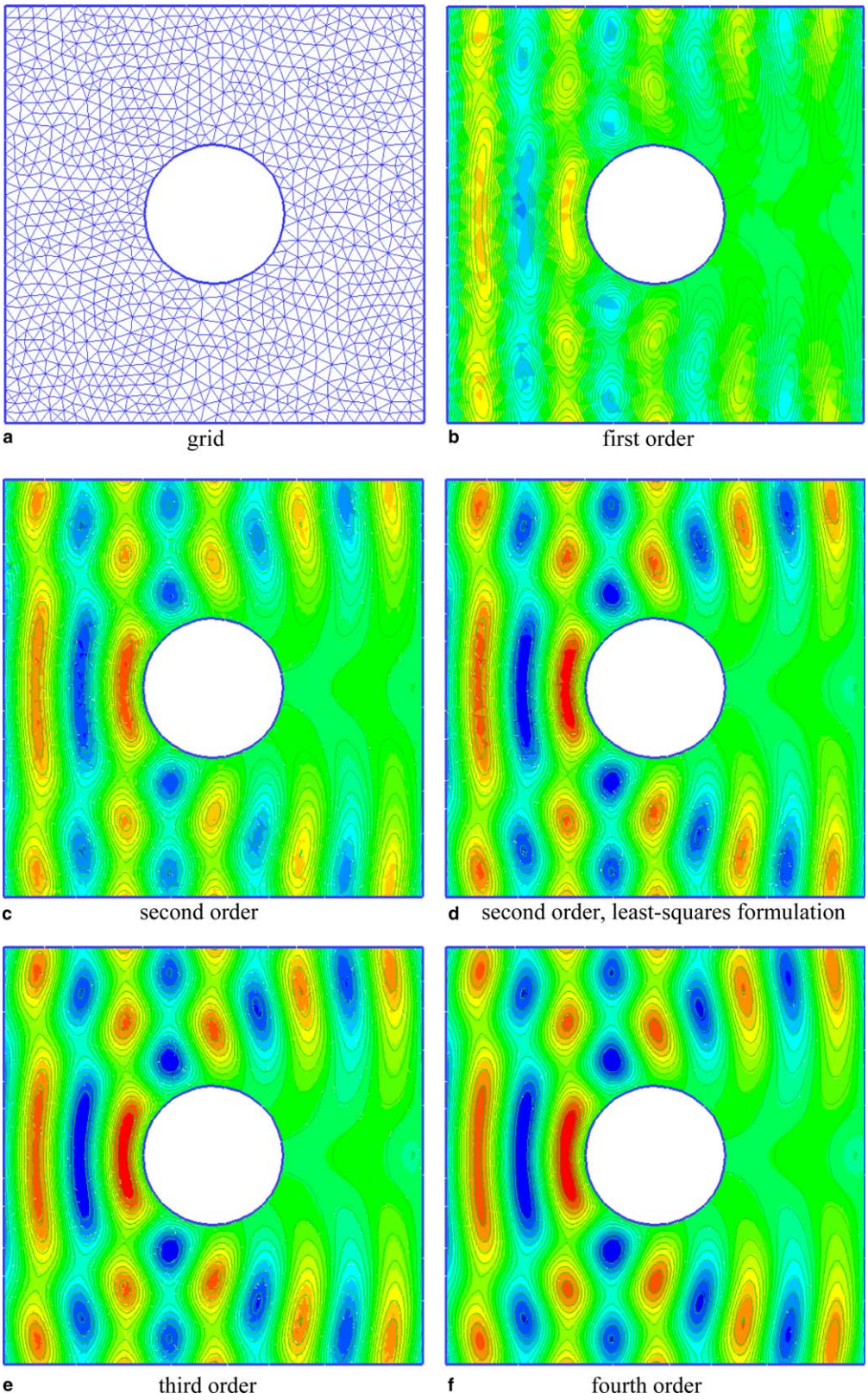

Fig. 9. Contour plot of E_z for a plane wave ($ka = 5$) incident on a perfectly conducting cylinder.

$$\frac{\partial \mathbf{D}}{\partial t} - \nabla \times \mathbf{H} = 0, \tag{41a}$$

$$\frac{\partial \mathbf{B}}{\partial t} + \nabla \times \mathbf{E} = 0. \tag{41b}$$

The electric and magnetic flux density vectors $(\mathbf{D}, \mathbf{B})$ and the intensity vectors $(\mathbf{E}, \mathbf{H})$ are related through the constitutive relations

$$\mathbf{D} = \varepsilon \mathbf{E}, \tag{42a}$$

$$\mathbf{B} = \mu \mathbf{H}, \tag{42b}$$

where ε is the permittivity and μ is the permeability of the material. Exact solutions exist for plane waves incident on simple bodies in two and three dimensions. The details of the time integration scheme, Riemann solver, and non-reflecting boundary procedure used here may be found in [26,28].

For the first test case, we considered a plane wave incident on a perfectly conducting circular cylinder. Calculations were carried out over an unstructured grid consisting of 2024 cells, shown in Fig. 9a. The cylinder is approximated with a 32-sided polygon. The outer boundary is two radii away from the body surface, with no

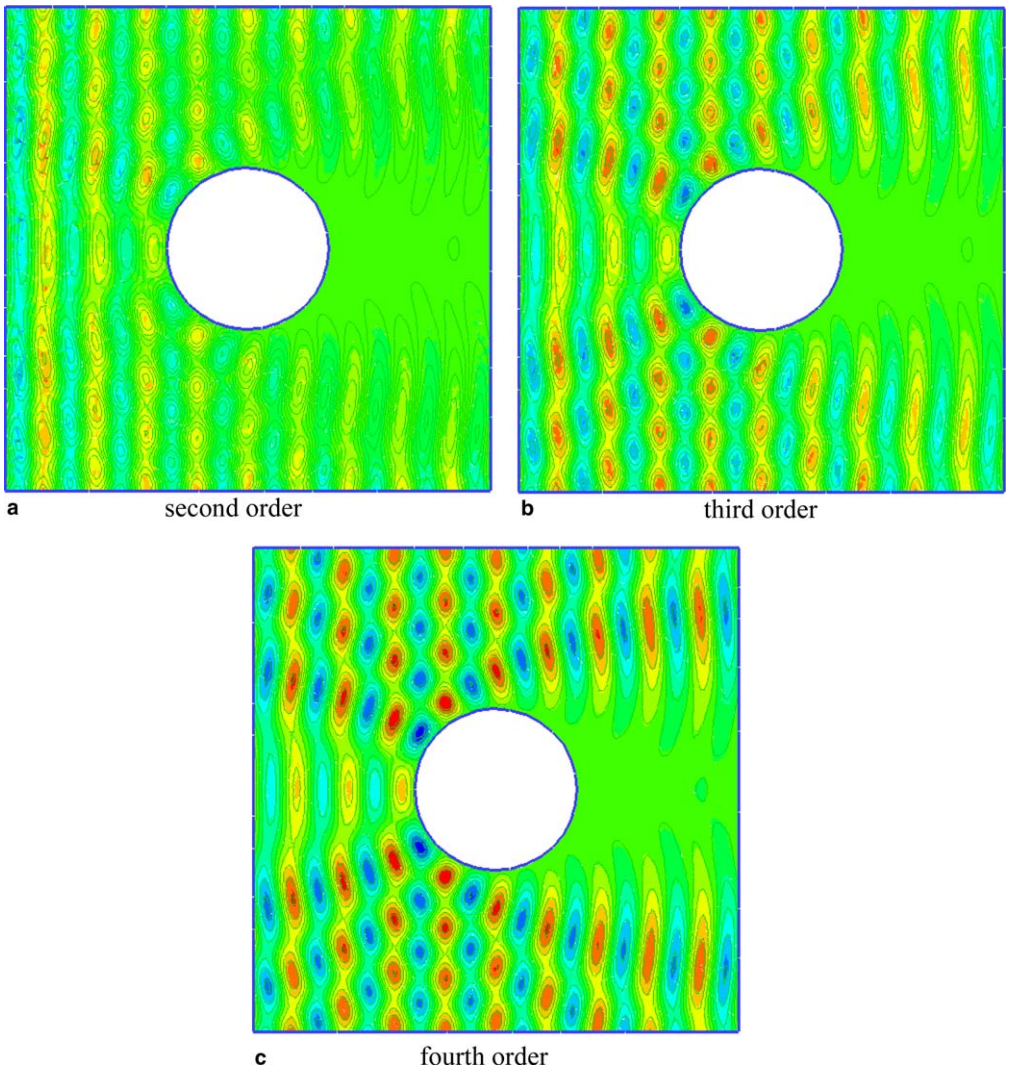

Fig. 10. Contour plot of E_z for a plane wave ($ka = 10$) incident on a perfectly conducting cylinder.

PML (perfectly matched layer). This gives approximately $30/ka$ cells per wavelength, or approximately $30\sqrt{n(n+1)}/ka$ unknowns per wavelength. Here k is the wave number, a is the radius of the cylinder, and $n = p + 1$ is the order of the accuracy of the method. The incident wave with $ka = 5$ is propagating from left to right. Figs. 9b–f show contour plots of E_z for a TM (transverse magnetic) wave as calculated using the first to fourth-order SD schemes with the u and F placements given in Figs. 4a, c and e–g. We have also plotted the exact solution (solid lines) on the same figures for easy comparisons. It is seen that the first-order solution is very dissipative with this resolution. While both second-order solutions captured all the main features of the wave, the scheme using the least-squares formulation is more accurate. The third and fourth-order solutions show an excellent agreement with the exact solution. Similar results were obtained for a TE (transverse electric) wave also. Figs. 10a–c show the contour plots for a wave with $ka = 10$ using the second to fourth-order SD schemes. With the grid resolution per wave length reduced by a factor of 2, the second-order scheme now is unable to produce an accurate solution. The third-order scheme can still capture the main features of the wave, but is a little bit too dissipative. Nevertheless, the fourth-order scheme agrees very well with the exact solution. We next tested the SD schemes on a grid in which the outer boundary is much closer to the body. Fig. 11a shows a grid consisting of 226 cells with the same resolution, but the outer boundary is only a half radius away from the body. Numerical solutions of the third and fourth-order SD schemes are plotted in Fig. 11b and c, respectively. They agree well with the exact solution.

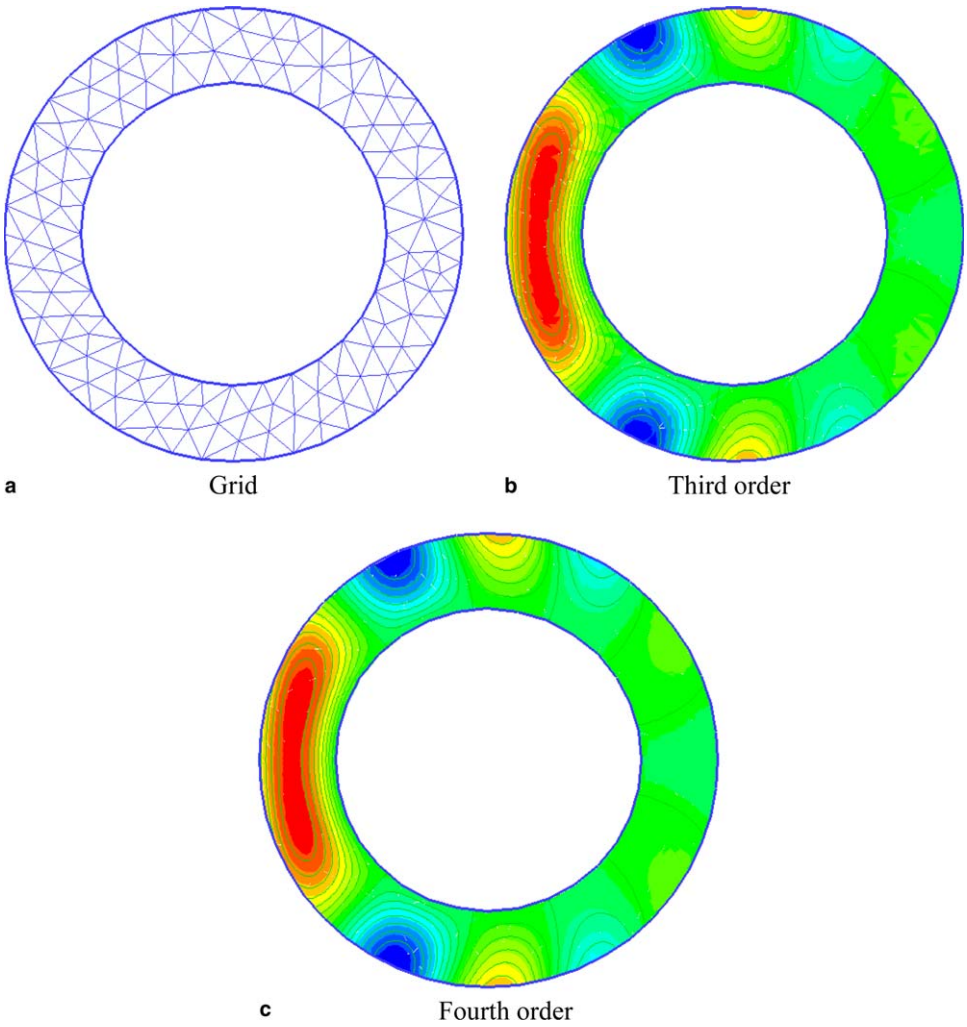

Fig. 11. Contour plot of E_z for a plane wave ($ka = 5$) incident on a perfectly conducting cylinder.

5. Concluding remarks

In this paper, we presented a new, high-order, conservative, and efficient method for conservation laws on unstructured grids. The method combines the best features of structured and unstructured grid methods in which the structured distribution of discrete variables in each unstructured cell maintains computational efficiency and geometric flexibility. It utilizes the concept of discontinuous and high-order local representations to achieve conservation and high accuracy. Universal reconstructions are obtained by distributing unknown and flux points in a geometrically similar manner for all unstructured cells. The flux derivatives needed to update the conservative unknowns are expressed as universal weighted sums of the fluxes, leading to great computational efficiency. An important aspect of the method is that the number of Riemann solvers per unknown decreases as the order of accuracy increases, reducing the cost for higher order. Placements of the unknown and flux points with various orders of accuracy are given for triangular elements. Accuracy studies of the method are carried out with the two-dimensional linear wave equation and Burgers' equation, and each order of accuracy is numerically verified. Numerical solutions of plane electromagnetic waves incident on perfectly conducting circular cylinders are presented and compared with the exact solutions to demonstrate the capability of the method. Excellent agreements have been found. Further improvements include extension to three dimensions, higher orders of accuracy, curved boundaries, optimization of unknown and flux placements, implicit time integration, grid and order adaptation, multidimensional limiters and filters, moving grids, and ultimately to the Euler and Navier–Stokes equations.

References

[1] T.J. Batina, A gridless Euler/Navier–Stokes solution algorithm for complex aircraft applications, AIAA paper No. 93-0333, 1993.
[2] J. Barth, P.O. Frederickson, High-order solution of the Euler equations on unstructured grids using quadratic reconstruction, AIAA Paper No. 90-0013, 1990.
[3] R. Beam, R.F. Warming, An implicit finite-difference algorithm for hyperbolic systems in conservation law form, J. Comput. Phys. 22 (1976) 87–110.
[4] J.A. Benek, J.L. Steger, F.C. Dougherty, A flexible grid embedding technique with application to the Euler equations, AIAA Paper No. AIAA-83-1944-CP, 1983.
[5] C. Canuto, M.Y. Hussaini, A. Quarteroni, T.A. Zang, Spectral Methods in Fluid Dynamics, Springer-Verlag, New York, 1987.
[6] Q. Chen, I. Babuska, Approximate optimal points for polynomial interpolation of real functions in an interval and in a triangle, Comput. Methods Appl. Mech. Engrg. 128 (1995) 405–417.
[7] Q. Chen, I. Babuska, The optimal symmetrical points for polynomial interpolation of real functions in the tetrahedron, Comput. Methods Appl. Mech. Engrg. 137 (1996) 89–94.
[8] K.C. Chung, A generalized finite difference method for heat transfer problems of irregular geometries, Numer. Heat Transfer 4 (1981) 345–357.
[9] B. Cockburn, C.-W. Shu, TVB Runge–Kutta local projection discontinuous Galerkin finite element method for conservation laws II: general framework, Math. Comput. 52 (1989) 411–435.
[10] B. Cockburn, S.-Y. Lin, C.-W. Shu, TVB Runge–Kutta local projection discontinuous Galerkin finite element method for conservation laws III: one-dimensional systems, J. Comput. Phys. 84 (1989) 90–113.
[11] B. Cockburn, S. Hou, C.-W. Shu, TVB Runge–Kutta local projection discontinuous Galerkin finite element method for conservation laws IV: the multidimensional case, Math. Comput. 54 (1990) 545–581.
[12] B. Cockburn, C.-W. Shu, The Runge–Kutta discontinuous Garlerkin method for conservation laws V: multidimensional systems, J. Comput. Phys. 141 (1998) 199–224.
[13] M. Delanaye, Y. Liu, Quadratic reconstruction finite volume schemes on 3D arbitrary unstructured polyhedral grids, AIAA Paper No. 99-3259-CP, 1999.
[14] D. Gottlieb, S.A. Orszag, Numerical Analysis of Spectral Methods: Theory and Applications, Society for Industrial and Applied Mathematics, Philadelphia, 1977.
[15] J.S. Hesthaven, From electrostatics to almost optimal nodal sets for polynomial interpolation in a simplex, SIAM J. Numer. Anal. 35 (1998) 655–676.
[16] J.S. Hesthaven, P.G. Dinesen, J.P. Lynov, Spectral collocation time-domain modeling of diffractive optical elements, J. Comput. Phys. 155 (1999) 287–306.
[17] J.S. Hesthaven, T. Warburton, Nodal high-order methods on unstructured grids I: time-domain solution of Maxwell's equations, J. Comput. Phys. 181 (2002) 186–221.
[18] T.J.R. Hughes, The Finite Element Method, Linear Static and Dynamic Finite Element Analysis, Prentice-Hall, Inc., 1987.
[19] A. Jameson, W. Schmidt, E. Turkel, Numerical solutions of the Euler equations by finite volume methods using Runge–Kutta time stepping schemes, AIAA paper No. 81-1259, 1981.
[20] G.E. Karniadakis, S.J. Sherwin, Spectral/hp Element Methods for CFD, Oxford University Press, 1999.

[21] D.A. Kopriva, A spectral multidomain method for the solution of hyperbolic systems, Appl. Numer. Math. 2 (1986) 221–241.
[22] D.A. Kopriva, A conservative staggered-grid Chebyshev multidomain method for compressible flows, J. Comput. Phys. 125 (1996) 244–261.
[23] D.A. Kopriva, A conservative staggered-grid Chebyshev multidomain method for compressible flows. II. Semi-structured method, J. Comput. Phys. 128 (1996) 475–488.
[24] D.A. Kopriva, A staggered-grid multidomain spectral method for the compressible Navier–Stokes equations, J. Comput. Phys. 143 (1998) 125–158.
[25] K.Z. Korczak, A.T. Patera, An isoparametric spectral element method for solution of the Navier–Stokes equations in complex geometries, J. Comput. Phys. 62 (1986) 361–382.
[26] Y. Liu, A generalized finite volume algorithm for solving Maxwell's equations on arbitrary grids, in: Proceedings of 10th Annual Review of Progress in Applied Computational Electromagnetics, 1994.
[27] Y. Liu, M. Vinokur, Exact integration of polynomials and symmetric quadrature formulas over arbitrary polyhedral grids, J. Comput. Phys. 140 (1998) 122–147.
[28] Y. Liu, M. Vinokur, Z.J. Wang, Spectral (finite) volume method for conservation laws on unstructured grids. V: Extension to three-dimensional systems, J. Comput. Phys. 212 (2006) 454–472.
[29] R.W. MacCormack, A.J. Paullay, Computational efficiency achieved by time splitting of finite difference operators, AIAA Paper No, 72-154, 1972.
[30] S.A. Orszag, Numerical simulation of incompressible flows within simple boundaries: I. Galerkin (spectral) representations, Stud. Appl. Math. 50 (1971) 293–327.
[31] A.T. Patera, A spectral element method for fluid dynamics: laminar flow in a channel expansion, J. Comput. Phys. 54 (1984) 468–488.
[32] W.H. Reed, T.R. Hill, Triangular mesh methods for the neutron transport equation, Tech. Report LA-UR-73-749, Los Alamos, Scientific Laboratory, 1973.
[33] P.L. Roe, Approximate Riemann solvers, parameter vectors, and difference schemes, J. Comput. Phys. 43 (1981) 357–372.
[34] V.V. Rusanov, Calculation of interaction of non-steady shock waves with obstacles, J. Comput. Math. Phys. USSR 1 (1961) 267–279.
[35] C.-W. Shu, Total-variation-diminishing time discretizations, SIAM J. Sci. Stat. Comput. 9 (1988) 1073.
[36] D. Sridar, N. Balakrishnan, An upwind finite difference scheme for meshless solvers, J. Comput. Phys. 189 (2003) 1–29.
[37] J.L. Steger, R.F. Warming, Flux vector splitting of the inviscid gasdynamics equations with applications to finite difference methods, J. Comput. Phys. 40 (1981) 263.
[38] M.A. Taylor, B.A. Wingate, R. Vincent, An algorithm for computing Fekete points in the triangle, SIAM J. Numer. Anal. 38 (2000) 1707–1720.
[39] M. Vinokur, Conservation equations of gasdynamics in curvilinear coordinate systems, J. Comput. Phys. 14 (1974) 105–125.
[40] Z.J. Wang, Spectral (finite) volume method for conservation laws on unstructured grids I: Basic formulation, J. Comput. Phys. 178 (2002) 210–251.
[41] Z.J. Wang, Y. Liu, Spectral (finite) volume method for conservation laws on unstructured grids II: Extension to two-dimensional scalar equation, J. Comput. Phys. 179 (2002) 665–697.
[42] Z.J. Wang, Y. Liu, Spectral (finite) volume method for conservation laws on unstructured grids III: One-dimensional systems and partition optimization, J. Scientific Comput. 20 (2004) 137–157.
[43] Z.J. Wang, L. Zhang, Y. Liu, Spectral (finite) volume method for conservation laws on unstructured grids IV: Extension to two-dimensional systems, J. Comput. Phys. 194 (2004) 716–741.
[44] S. Wolfram, The Mathematica Book, fourth ed., Wolfram Media and Cambridge University Press, New York, 1999.